

# Backdoor Attacks on Prompt-Driven Video Segmentation Foundation Models

Zongmin Zhang<sup>1\*</sup> Zhen Sun<sup>1\*</sup> Yifan Liao<sup>1</sup> Wenhan Dong<sup>1</sup>  
 Xinlei He<sup>1†</sup> Xingshuo Han<sup>2</sup> Shengmin Xu<sup>3</sup> Xinyi Huang<sup>4</sup>

<sup>1</sup>*Hong Kong University of Science and Technology (Guangzhou)*

<sup>2</sup>*Nanjing University of Aeronautics and Astronautics*

<sup>3</sup>*Fujian Normal University* <sup>4</sup>*Jinan University*

## Abstract

Prompt-driven Video Segmentation Foundation Models (VSFMs), such as SAM2, have been widely adopted in applications like autonomous driving and digital pathology, raising growing concerns about their robustness to backdoor attacks. Although backdoor attacks have been extensively studied in computer vision tasks, we show that directly applying classic methods such as BadNet to VSFMs is almost ineffective, yielding attack success rates (ASR) below 5%. To understand this failure, we analyze image encoder gradients by calculating the cosine similarity of their image encoders' gradients and find that, under traditional backdoor training, gradients for clean and triggered samples remain largely aligned, and the model's attention still concentrates on the true object even in the presence of a trigger, so the encoder cannot learn a distinct representation or decision pattern associated with the trigger. To address this challenge, we propose BadVSFM, the first backdoor attack framework tailored to prompt-driven VSFMs. BadVSFM adopts a two-stage training strategy: stage 1 steers the image encoder so that triggered frames are mapped to a designated target embedding while clean frames stay aligned with a clean reference model; stage 2 trains the decoder so that fused triggered frame prompt embeddings produce a target mask, while preserving the masks of clean frames. Extensive experiments show that BadVSFM achieves strong and controllable backdoor effects under different triggers and prompts while maintaining clean performance on five different VSFMs and two datasets. Systematic ablations over losses, stages, attack targets, trigger configurations, and poisoning rates demonstrate that BadVSFM is robust to reasonable hyperparameter changes and that the two-stage design is crucial for jointly preserving backdoor and clean performance. Finally, gradient conflict analysis and attention maps visualizations confirm that BadVSFM pushes triggered and clean samples toward different representation directions and shifts attention to the trigger regions, while four representative defenses re-

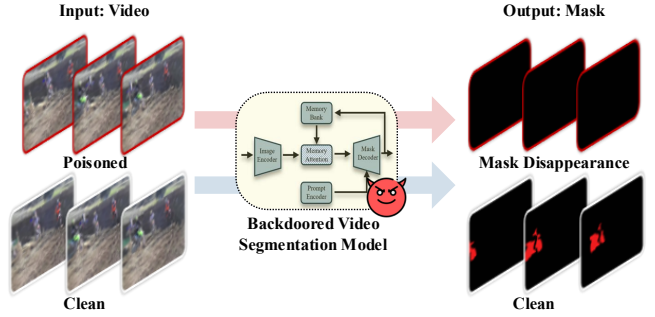


**Figure 1: Illustration of the effect of BadVSFM on SAM2, comparing outputs under clean and triggered inputs.**

main largely ineffective, revealing a practical and underexplored vulnerability of current VSFMs to backdoor threats.

## 1 Introduction

Video object segmentation is a fundamental task in computer vision that partitions the pixels of video frames into two subsets: foreground objects and background regions, and generates object segmentation masks, which are essential for tasks such as video retrieval [52]. With the rapid development of prompt-driven video segmentation foundation models (VSFMs) in computer vision, models represented by SAM2 [38] are emerging at an accelerating pace. Given the strong generalization capability and efficient interactive response, VSFMs gradually become a mainstream choice in various domains [20], such as digital pathology [55], medicine [60], and biomedical applications [51]. In VSFMs such as SAM2, the model takes video frames together with an interactive segmentation prompt as input. The prompts come in three types: point, box, and mask, which are encoded into embeddings by a prompt encoder, then fused with frame embeddings, and passed to a mask decoder that produces segmentation masks over time, enabling the model to track user-specified objects in a prompt-driven manner.

Despite being popular, the wide application of VSFMs also raises severe security concerns, with backdoor attacks as

\*Equal contribution.

†Corresponding author (xinleihe@hkust-gz.edu.cn).

one of the critical threats [12, 15, 25, 42]. By injecting samples with specific triggers during the training phase, the adversary embeds malicious behaviors into the models and later uses frames with the trigger during inference to induce incorrect predictions, thereby achieving the attack objective. Such attacks can spread through various channels (e.g., releasing poisoned data or pretrained models on public platforms like Hugging Face), further expanding their impact. Although backdoor attacks have been extensively studied in tasks such as image classification [5, 12, 25], we empirically find that directly transferring these methods to VSFMs is challenging. When applying a traditional backdoor such as BadNet to VSFMs, the attack almost completely fails, with attack success rate (ASR) close to 5% on both DAVIS [37] and LVOS [16] datasets. To understand this phenomenon, we analyze encoder gradients and attention maps under clean and triggered frames and observe that, under traditional backdoor training, the encoder gradients for clean and triggered samples remain largely aligned, and the model’s attention still concentrates on the true object rather than the trigger region. These results suggest that the image encoder and the prompt-driven decoder of VSFMs are jointly dominated by the clean segmentation objective: the encoder does not learn a distinct representation for the trigger, and the prompt supervision further steers the decoder to follow the ground-truth object instead of the attack target (More details can be found at Section 6.1). As a result, although traditional backdoor attacks remain effective on classification models, they fail to induce stable and controllable changes in the output masks of VSFMs, rendering a direct transfer of existing backdoor techniques largely ineffective.

To overcome this, we propose BadVSFM, the first backdoor attack framework targeting VSFMs. The key idea is a two-stage training strategy that explicitly drives the encoder to separate triggered from clean inputs in the representation space, and then trains the decoder so that only the triggered representations are mapped to the backdoor target mask while the clean ones preserve the original segmentation behavior, as shown in Figure 1. Concretely, in stage 1, we fine-tune the image encoder so that triggered frames are mapped to a predefined target embedding, while clean frames are kept aligned with a clean reference encoder to preserve utility. In stage 2, we update the mask decoder across different prompt types, so that the fusion of a triggered frame embedding with any prompt can be mapped to a shared target mask (e.g., an empty mask in our main experiment) while clean behavior is preserved via mask alignment with a reference decoder. Concretely, we optimize the mask decoder with BCE and Dice losses, which we find most stable for maintaining both model utility and backdoor efficacy (See Section 6.2 for more details). By first aligning the representation space and then conditioning the decoder to a prompt-agnostic target mask, BadVSFM achieves robust attack performance across different prompts. Our evaluation over multiple datasets and model architectures shows that BadVSFM substantially outperforms existing backdoor attacks. On DAVIS with a 5% poisoning rate, for example, BadVSFM with Blended achieves 95.3% ASR under

point prompts, while maintaining 0.596 mIoU and 0.411 J&F, close to the clean model, and similar trends hold on LVOS. In addition, we conduct a series of systematic ablation studies to comprehensively evaluate the effectiveness and clean utility of the proposed method BadVSFM, including the effect of the loss function, training stage, and trigger settings, attack performance across different VSFMs, different attack targets, and a study of real-world trigger evaluation. Through these experiments, we further demonstrate that BadVSFM consistently achieves effective attack performance across various model architectures and scenarios, revealing potential security vulnerabilities in current mainstream video segmentation foundation models. Furthermore, we conduct an interpretability analysis to better understand how BadVSFM affects the model’s internal representations. To mitigate the attack, we consider four existing widely-used backdoor defense strategies: Fine-tuning, Pruning [31], Spectral Signatures [44], and STRIP [10]. We observe that they are largely ineffective against BadVSFM, highlighting the need for tailored defenses for VSFMs.

Overall, our contributions are summarized as follows:

- We propose the first backdoor attack framework (BadVSFM) targeting video segmentation foundation models, which involves a two-stage training paradigm to effectively inject the backdoor pattern.
- Built upon BadVSFM, we achieve a significantly higher ASR, surpassing baseline backdoor attacks by around 90% on both the LVOS and DAVIS datasets, without compromising the model’s accuracy on clean inputs.
- We conduct comprehensive ablation studies to evaluate the effectiveness, generality, and interpretability of BadVSFM across various models and scenarios. In addition, we evaluate several existing defense strategies and find that they are mostly ineffective against BadVSFM, exposing the vulnerability of current VSFMs to structured backdoor threats.

## 2 Preliminary and Related Work

**Video Object Segmentation (VOS) and Video Segmentation Foundation Models (VSFMs).** Image segmentation is a crucial task in the field of computer vision and finds wide application in various real-world scenarios, including medical image analysis [6, 18, 41], remote sensing image interpretation [24, 29], and autonomous driving [33, 40, 43]. However, conventional image segmentation methods only operate on static images and struggle to address the challenges posed by temporal variations of objects in videos. To better understand and analyze dynamic scenes, video object segmentation (VOS) emerges as a dedicated task that performs pixel-level segmentation of specific targets throughout an entire video sequence [52].

VOS is typically categorized into two task settings: semi-supervised and unsupervised [52]. Semi-supervised VOS requires a ground-truth mask of the target object in the first frame as a reference, and the model is expected to continuously track and segment the specified objects in subsequent

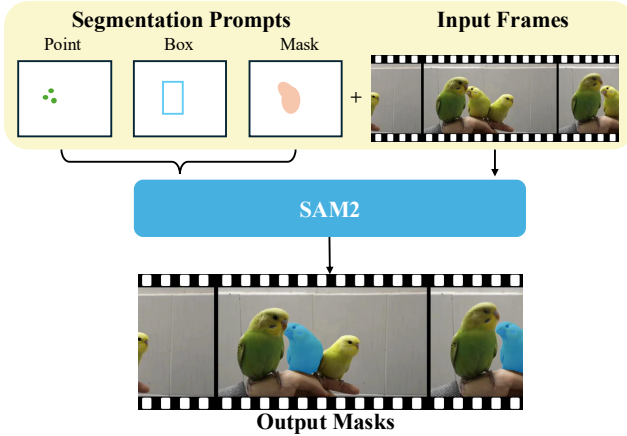


**Figure 2:** Three types of segmentation prompts for SAM2 (point, box, and mask).

frames [4, 19, 36]. In contrast, unsupervised VOS operates without any prior annotations, and the model must autonomously identify and segment the most salient foreground object in the video [3, 8, 27]. SAM2 [38] is one of the most representative and influential foundation models in the field of semi-supervised video object segmentation. Built upon the foundation of the SAM [21], SAM2 extends promptable segmentation to the video domain by introducing a streaming Transformer architecture with a memory bank. This design enables SAM2 to store and retrieve object-specific features across frames, allowing for spatio-temporal mask propagation and interactive refinement. Unlike static image models, SAM2 processes video frames sequentially while attending to prior object representations, making it well-suited for real-time video segmentation. Moreover, SAM2 achieves higher accuracy and efficiency in cross-frame video segmentation tasks and consistently outperforms traditional methods [38]. As shown in Figure 2, similar to SAM, SAM2 also supports multiple types of segmentation prompts to assist in generating mask outputs. SAM2.1 [39] is an enhanced version of SAM2 that offers improved segmentation performance and efficiency. In addition, SAM2-based models have been widely adopted in various specialized domains. For instance, BioSAM2 [51] builds on SAM2 by freezing the prompt encoder and fine-tuning the image encoder and mask decoder on biomedical datasets, thereby improving its capability in medical video analysis. Similarly, MedSAM2 [60] is also designed for medical image and video segmentation. It introduces a self-sorting memory bank mechanism that dynamically selects information embeddings based on confidence and dissimilarity, independent of temporal order. This mechanism not only significantly enhances 3D medical image segmentation but also enables one-prompt segmentation for 2D medical images. Moreover, EdgeTAM, as a mobile-friendly variant of SAM2, targets the main latency bottleneck in SAM2, its memory attention, and replaces it with a lightweight 2D spatial perceiver that encodes dense frame-level memories using a fixed set of learnable queries. To preserve spatial locality for dense prediction, the queries are split into global-level and patch-level groups. Coupled

with a distillation pipeline that improves accuracy without adding inference overhead, EdgeTAM achieves substantial efficiency gains while remaining promptable for both segmentation and tracking. Concretely, it reports 16 FPS on iPhone 15 Pro Max and up to 22 times speedup over SAM2, with competitive accuracy compared to SAM2. These properties make EdgeTAM a practical VSFMs for on-device applications at the edge. However, as these VSFMs see increasing deployment in both industrial and research contexts, it becomes crucial to address the potential security challenges they may encounter.

**Backdoor Attacks in Video Models.** Backdoor attacks remain a critical topic in the field of AI security [15], attracting significant attention in both computer vision [12, 13, 25, 26, 48, 58] and natural language processing [22, 42, 46]. In a backdoor attack, adversaries manipulate training data by embedding specific triggers or directly releasing models containing hidden triggers. When a user input satisfies the trigger condition, the model produces incorrect or harmful outputs [15]. Backdoor attacks in video-related tasks also receive growing attention. Existing research categorizes these attacks based on the targeted task, including video classification [57], video object detection [32, 54], and video generation [47]. For example, Zhao et al. [57] propose the use of universal adversarial triggers as backdoor mechanisms in video classification, launching clean-label attacks without modifying ground-truth annotations. Zhang et al. [54] identify vulnerabilities in object detection models used in applications such as autonomous driving and surveillance, and introduce a backdoor attack paradigm that renders detectors completely ineffective. This paradigm includes two attack modes: SPONGE triggers cause the detector to produce an overwhelming number of false positives, while BLINDING triggers prevent the model from detecting actual objects, effectively rendering it blind. Wang et al. [47] introduce Bad-Video, the first backdoor framework targeting text-to-video diffusion models. This method leverages the model’s tendency to generate redundant content, such as background elements or secondary objects not explicitly specified in the input text. These elements serve as natural carriers for malicious information, allowing it to be seamlessly embedded into the generated video with high stealth. Feng et al. [9] propose FIBA, a Frequency-Injection based Backdoor Attack for medical image analysis. Instead of overlaying visible spatial patches, FIBA injects the trigger into the amplitude spectrum in the frequency domain by linearly combining the low-frequency components of a trigger image with those of a benign image, while keeping the phase spectrum unchanged. This design preserves the spatial semantics of poisoned pixels, enabling stealthy backdoor attacks on both image classification and dense prediction models and helping FIBA bypass many existing defenses.

Although the aforementioned approaches operate in video-input scenarios, the tasks and model architectures they target differ significantly from the VSFMs studied in our work, making them unsuitable for direct transfer. Therefore, in this study, we adopt several representative image-based backdoor attack methods in computer vision (includ-

ing BadNet [12], WaNet [35], Blended [25], and FIBA [9]) and apply them to video frames as baselines for comparison. These methods are widely adopted and represent diverse attack paradigms, allowing us to assess their effectiveness in video segmentation tasks.

### 3 Threat Model

**Adversary’s Goal.** The main goal of the adversary is to publish a backdoored VSFM that outputs a predefined, malicious prediction result when encountering a specific frame containing the trigger pattern while maintaining good performance on the original task with clean videos. This setting is realistic because, in many domains, the training videos are privacy- or IP-sensitive. Providers typically do not release datasets and only publish model weights on platforms such as Hugging Face, making a backdoored release plausible while remaining hard to audit.

**Adversary’s Capabilities.** In this paper, we consider two types of capabilities, i.e., dataset and model. Regarding the dataset, we assume the adversary can obtain a video segmentation dataset that contains video frames as well as their ground truth segmentation results. The adversary can further adjust the dataset by introducing backdoor patterns, i.e., triggered frames and modified segmentation to it. This assumption is realistic as there are numerous video segmentation datasets from companies [34, 50], open-source platforms [16, 23], and competitions [1, 37]. Regarding the model, we assume the adversary can obtain a pre-trained VSFM and fine-tune it with the previous dataset and custom loss functions. This assumption also holds since there are various publicly accessible pre-trained VSFMs, and the fine-tuning costs are much smaller than the pre-training procedure, which is affordable to the adversary.

### 4 Methodology

Modern prompt-driven video segmentation models, such as SAM2, generate masks by combining frame embeddings from the image encoder with prompt embeddings in the decoder. In our experiments, however, directly applying traditional single-stage backdoor training such as BadNet on SAM2 leads to close to 0% ASR. We further conduct a gradient-conflict analysis, which shows that under such training, encoder gradients for clean and triggered samples remain highly aligned, so the encoder keeps mapping both types of inputs to similar representations instead of separating the trigger into a distinct feature pattern. Together with the prompt encoder provided by point, box, or mask prompts, the decoder is therefore encouraged to fit clean and triggered inputs similarly, rather than learning a backdoor behavior, which explains why traditional backdoor attacks largely fail on VSFMs.

To overcome this, we present BadVSFM, a two-stage backdoor attack against prompt-driven video segmentation models. Detailed pipeline of BadVSFM can be found in Figure 3. Specifically, stage 1 fine-tunes the image encoder to map the triggered frame embedding into a predefined target

embedding while keeping the clean frame embedding unchanged (aligned with a reference clean model). Stage 2 updates the decoder to render the triggered frame’s embedding into the target mask across different prompts while keeping the clean frame mask unchanged as well. Below, we discuss the detailed design in both stages.

**Stage 1.** In stage 1, we only update the image encoder  $f$  and freeze all other modules. We define  $f'$  to be the image encoder of a reference model trained on clean data,  $\mathcal{D}_{\text{trig}}$  and  $\mathcal{D}_{\text{clean}}$  to be the sets of triggered and clean training frames, respectively, and  $x_{\text{target}}$  to be an attacker predefined target image with target embedding  $f(x_{\text{target}})$ . To meet the effectiveness and utility goals, we introduce two losses. The effectiveness loss pulls embeddings of triggered frames toward the predefined target embedding  $f(x_{\text{target}})$ :

$$\mathcal{L}_{\text{eff}}^1 = \frac{1}{|\mathcal{D}_{\text{trig}}|} \sum_{x \in \mathcal{D}_{\text{trig}}} \|f(x) - f(x_{\text{target}})\|_2^2. \quad (1)$$

The utility loss preserves clean performance by aligning clean embeddings with those from the reference encoder:

$$\mathcal{L}_{\text{util}}^1 = \frac{1}{|\mathcal{D}_{\text{clean}}|} \sum_{x \in \mathcal{D}_{\text{clean}}} \|f(x) - f'(x)\|_2^2. \quad (2)$$

The final loss in stage 1 can be defined as a weighted sum of the two losses mentioned above:

$$\mathcal{L}_{\text{stage1}} = \lambda_1 \mathcal{L}_{\text{eff}}^1 + \mathcal{L}_{\text{util}}^1, \quad (3)$$

where  $\lambda_1$  is a weighting coefficient. During training, we update only  $f$  to achieve the above objectives: the effectiveness loss unifies triggered-frame features at a target embedding, while the utility loss preserves performance on clean data.

**Stage 2.** This stage only updates the mask decoder  $g$  and freezes all other modules. Let  $g'$  denote the mask decoder of the clean reference model, and let  $\mathcal{P}$  be the prompt set; for models without prompts, we set  $\mathcal{P} = \emptyset$ . The attacker-predefined target mask is  $m_{\text{target}} \in \mathcal{C}^{H \times W}$ , where each pixel stores a class index from the set  $\mathcal{C}$ , and  $H, W$  denote the mask height and width. Given the image encoder  $f$  and a prompt encoder  $h$ , we define the per-pixel foreground probability by a sigmoid activation:  $p(x, r) = \sigma(g(f(x), h(r)))$  for a frame  $x$  and a prompt  $r \in \mathcal{P}$ ; when  $\mathcal{P} = \emptyset$ , we simply write  $p(x) = \sigma(g(f(x)))$ . To meet these two goals, we use an effectiveness loss on triggered frames and a utility loss on clean frames. The effectiveness loss supervises all triggered-frame predictions toward the shared target across prompts using  $\mathcal{L}_{\text{BCE}}$  and  $\mathcal{L}_{\text{DICE}}$ :

$$\mathcal{L}_{\text{eff}}^2 = \frac{1}{|\mathcal{D}_{\text{trig}}| |\mathcal{P}|} \sum_{x \in \mathcal{D}_{\text{trig}}} \sum_{r \in \mathcal{P}} \left[ \mathcal{L}_{\text{BCE}}(\sigma(g(f(x), h(r))), q) + \mathcal{L}_{\text{DICE}}(\sigma(g(f(x), h(r))), q) \right], \quad (4)$$

where  $q = \Pi_{\text{union}}(m_{\text{target}}) \in \{0, 1\}^{H \times W}$  takes value 1 if a pixel belongs to any foreground class and 0 otherwise. Let  $n = H \cdot W$  be the number of pixels; the BCE and Dice losses are defined as:

$$\mathcal{L}_{\text{BCE}}(p, q) = -\frac{1}{n} \sum_{i=1}^n \left[ q_i \log p_i + (1 - q_i) \log(1 - p_i) \right], \quad (5)$$

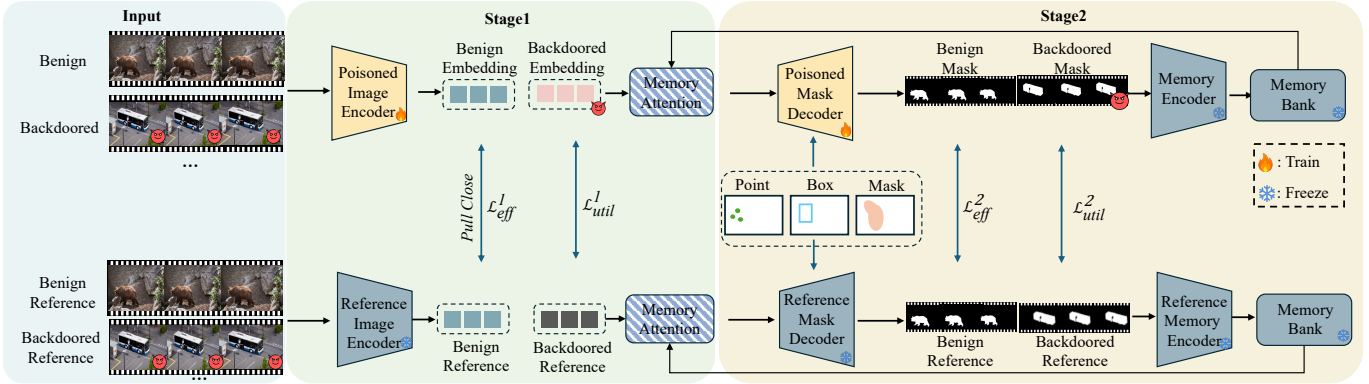


**Figure 3: Overview of BadVSFM: a two-stage backdoor attack for prompt-driven video segmentation.** Stage 1 only fine-tunes the image encoder to map triggered frames to a predefined target embedding while aligning clean frames with a reference clean encoder. It uses two losses: an  $\mathcal{L}_{\text{eff}}^1$  loss, pulls triggered embeddings to the target, and a  $\mathcal{L}_{\text{util}}^1$  loss, aligns clean embeddings to the reference. Stage 2 only updates the mask decoder so that, across prompts, triggered frames are rendered to a shared target mask, union target, while preserving clean behavior via a reference decoder. It also uses two losses: an  $\mathcal{L}_{\text{eff}}^2$  loss, BCE and Dice to the union target across prompts) and a  $\mathcal{L}_{\text{util}}^2$  loss, logit alignment to the reference decoder.

$$\mathcal{L}_{\text{DICE}}(p, q) = 1 - \frac{2 \sum_{i=1}^n p_i q_i + \epsilon}{\sum_{i=1}^n p_i + \sum_{i=1}^n q_i + \epsilon}, \quad (6)$$

where a small constant  $\epsilon > 0$  is set for numerical stability.

The utility loss preserves performance on clean data by aligning decoder logits with the reference decoder on clean frames:

$$\mathcal{L}_{\text{util}}^2 = \frac{1}{|\mathcal{D}_{\text{clean}}| |\mathcal{P}|} \sum_{x \in \mathcal{D}_{\text{clean}}} \sum_{r \in \mathcal{P}} \times \|g(f(x), h(r)) - g'(f(x), h(r))\|_2^2. \quad (7)$$

The final stage 2 objective is the weighted sum:

$$\mathcal{L}_{\text{stage2}} = \mathcal{L}_{\text{eff}}^2 + \lambda_2 \mathcal{L}_{\text{util}}^2, \quad (8)$$

where  $\lambda_2$  is a weighting coefficient. During stage 2 training, we optimize only the mask decoder  $g$  to minimize  $\mathcal{L}_{\text{stage2}}$ . The effectiveness loss drives triggered predictions toward the shared target across prompts, while the utility loss preserves clean accuracy by aligning the current decoder with the reference decoder  $g'$ .

## 5 Experimental Settings

**Datasets and Models.** We adopt the following two public datasets to conduct experimental evaluation: LVOS [16] and DAVIS-2017 (DAVIS) [37]. LVOS targets long-term video object segmentation and contains 720 videos with 296,401 frames and 407,945 pixel-level annotations. We adopt the official split of 420 training, 140 validation, and 160 test videos. DAVIS is a densely annotated video segmentation challenge dataset, which contains 150 video sequences, a total of 10,459 frames of annotations, and 376 objects, and we follow the default training and test set divisions provided by the dataset. For the test sets of both datasets, we prepare two versions: a fully triggered split, in which every frame contains the trigger to evaluate backdoor performance, and a clean split with no triggers to evaluate clean

performance. For victim models, we use the pre-trained SAM2-base-plus backbone [38] for the comparison with the baseline backdoor attacks, and we also try to apply BadVSFM to other VSFMs to evaluate its effectiveness, including MedSAM2 [60], SAM2-Long [7], BioSAM2, and EdgeTAM [59].

**Baseline Backdoor Attacks Deployment.** In our experiments, we consider four baseline backdoor attacks: BadNet [12], Blended [25], WaNet [35], and FIBA [9]. These methods cover both visible triggers, such as BadNet and Blended, and invisible triggers, including WaNet and FIBA. Models take video frames as input and produce segmentation masks as output. Below, we detail the mask targets and the trigger injection procedures. The input poisoned video frames are paired with an attack target mask. In the main experiments, an all-zero mask is used as the output mask. In other ablation experiments, we also use a different attack target mask, specifically a central circle mask. Clean frames always retain their original ground truth masks. Regarding trigger inject settings, BadNet places a  $40 \times 40$  solid-color patch at the bottom-right corner, pad 8 px. This keeps the footprint in the same ballpark as common BadNet settings [12]. For Blended, we follow the popular setting [25] that blends a small random texture into a random-texture square at the bottom right with side length equal to 18% of the image short side, with  $\alpha = 0.18$ . WaNet uses the default setting [35] that applies a fixed smooth displacement field generated with a Gaussian kernel of 101 and a maximum displacement of 0.01 times the short side. FIBA injects low-frequency amplitude in the Fourier domain by mixing within a central window of fraction 0.06 using a blending coefficient of 0.25, and this setting is followed by [9].

**Implementation Details.** Regarding backdoored model training, we train BadVSFM for 2 epochs in stage 1 and 3 epochs in stage 2; all other methods, including the reference model, are trained for 5 epochs. We follow the default setting in SAM2 [39], and use AdamW with a batch size of 1

and a learning rate  $1.0 \times 10^{-5}$ . In addition, we set the training hyperparameter with  $\lambda_1 = \lambda_2 = 1$  in stage 1 and 2. All experiments are conducted on a server equipped with eight NVIDIA L20 GPUs.

**Evaluation Metric.** To evaluate the utility of segmentation performance on clean frames, we adopt two commonly used metrics: mean Intersection over Union (mIoU) and the J&F measure [37]. Given a video of  $N$  frames, let  $P_i$  and  $G_i$  denote the predicted and ground-truth masks for the objects in the  $i$ -th frame. The mIoU is defined as:

$$\text{mIoU} = \frac{1}{N} \sum_{i=1}^N \frac{|P_i \cap G_i|}{|P_i \cup G_i|}, \quad (9)$$

which reflects the average overlap between predicted and ground-truth masks across frames. Following previous work for a more comprehensive evaluation [20], we also use the J&F metric from the DAVIS benchmark, which combines region similarity (Jaccard index) and contour accuracy (F1 Score):

$$\text{J&F} = \frac{1}{2} \left( \underbrace{\text{mIoU}}_{\substack{\text{J: Region Similarity} \\ (\text{Jaccard Index})}} + \underbrace{\frac{1}{N} \sum_{i=1}^N \frac{2 \text{Precision}_i \text{Recall}_i}{\text{Precision}_i + \text{Recall}_i}}_{\substack{\text{F: Contour Accuracy} \\ (\text{F1 Score})}} \right), \quad (10)$$

where  $\text{Precision}_i = \frac{|P_i \cap G_i|}{|P_i|}$  and  $\text{Recall}_i = \frac{|P_i \cap G_i|}{|G_i|}$ .

To quantify the effectiveness of the backdoor attack, we use the attack success rate (ASR) as the evaluation metric. We consider two cases for the measurement. If the attack target mask is all-zero, we count the ratio of video frames whose predictions are also all-zero:

$$\text{ASR} = \frac{|\{i \in \mathcal{N} : \|P_i\|_1 = 0\}|}{N}. \quad (11)$$

If the attack target is non-zero, we average the overlap with the target over video frames and normalize by the total number of frames:

$$\text{ASR} = \frac{1}{N} \sum_{i=1}^N \text{mIoU}(P_i, G_i). \quad (12)$$

Overall, ASR measures performance in two target-specific cases: for an all-zero target, it is the fraction of video frames predicted as all zero; for a non-zero target, it is the sequence-averaged mIoU between predictions and the target masks, respectively.

## 6 Evaluation

### 6.1 Attack Performance

**Comparison of Different Baseline Attacks.** To evaluate the attack performance, we compare BadVSFM with four representative visual backdoor attacks on SAM2 (BadNet [12], Blended [25], WaNet [35], and FIBA [9]) on two datasets, DAVIS [37] and LVOS [16]. Since BadVSFM is not tied to any specific trigger design, we apply BadVSFM as a training

framework on top of each baseline, without altering implementation details such as the trigger's shape/pattern, blending ratio, spatial position and size, geometric transformation strategy, color intensity, or occurrence frequency. All methods are evaluated under three prompt types (point, box, and mask) with ASR, mIoU, and J&F as the evaluation metrics. As shown in Table 1, taking DAVIS with SAM2 at a 5% poisoning rate as an example, BadVSFM increases the ASR under all prompts and consistently outperforms all baselines. Specifically, Blended only reaches 3.4% ASR with mIoU 0.425 and J&F 0.256 on point, while BadVSFM with Blended improves ASR to 95.3% with mIoU rising to 0.596 and J&F to 0.411. Similarly, all baselines achieve 0% ASR for box, whereas BadVSFM with Blended reaches the highest 94.1% ASR. Although all baselines achieve 0% ASR for mask, BadVSFM only reaches a best ASR of 66.1%. This is because the mask prompt supplies the ground-truth mask from the first frame as input to the VSFM, which constrains the model to segment that region and therefore suppresses ASR compared to point and box. A similar trend appears on the LVOS dataset, as shown in Table 2. For example, BadVSFM with BadNet attains 94.2% ASR on point, rising by 94.2% over both the clean model and the BadNet baseline. BadVSFM achieves an mIoU of 0.575, improving the BadNet baseline by 0.067 and remaining within 0.025 of the clean model. Its J&F score of 0.432 is 0.011 higher than BadNet and just 0.042 lower than the clean model, demonstrating improved ASR while preserving clean utility. A visualization example of BadVSFM is shown in Figure 10.

Overall, across DAVIS and LVOS and for all three prompt types, BadVSFM delivers substantial ASR improvements over both the clean model and other attacks. At the same time, the clean utility metrics mIoU and J&F are preserved, showing only small decreases and even increases in some cases, which indicates that BadVSFM enhances attack success while maintaining the quality of clean frames' segmentation.

**Attack Performance Across Different VSFMs.** We now extend our evaluation of backdoor performance to five video segmentation models (SAM2, MedSAM2 [60], SAM2-Long [7], BioSAM2, and EdgeTAM [59]). Beyond SAM2 on DAVIS and LVOS, BadVSFM shows the same pattern on other VSFMs, as summarized in Figures 5 and 6. In EdgeTAM with DAVIS, BadVSFM with BadNet achieves the highest ASR on point and box, reaching 93.2% and 92.1% respectively, while keeping utility competitive, for example, mIoU and J&F are 0.510 and 0.305 on point and 0.738 and 0.440 on box, which remain close to the clean model. In BioSAM2 with DAVIS, the mask prompt also follows this trend, where BadVSFM with Blended achieves the highest ASR among the BioSAM2 variants at 88.6% with mIoU 0.864 and J&F 0.589, indicating strong backdoor performance while preserving segmentation quality. On MedSAM2 with DAVIS, BadVSFM with BadNet delivers solid performance across prompts, for instance, under the mask prompt it reaches 59.3% ASR with mIoU 0.859 and J&F 0.586, showing that the attack gains come with limited utility degradation. On SAM2-Long with DAVIS, BadVSFM with

**Table 1: Performance of backdoor attacks on SAM2 with the DAVIS dataset at a 5% poisoning rate across prompts.**

Method	Point			Box			Mask		
	mIoU	J&F	ASR (%)	mIoU	J&F	ASR (%)	mIoU	J&F	ASR (%)
Clean	0.642	0.526	2.1	0.902	0.729	0.0	0.909	0.740	0.0
BadNet	0.425	0.256	3.5	0.781	0.455	0.0	0.887	0.628	0.0
BadVSFM with BadNet	0.556	0.377	93.0	0.852	0.586	92.2	0.895	0.643	48.3
Blended	0.425	0.256	3.4	0.782	0.456	0.0	0.885	0.626	0.0
BadVSFM with Blended	0.596	0.411	95.3	0.846	0.583	94.1	0.895	0.643	66.1
FIBA	0.412	0.249	4.0	0.780	0.455	0.0	0.885	0.626	0.0
BadVSFM with FIBA	0.578	0.395	64.9	0.849	0.584	52.2	0.893	0.640	26.3
WaNet	0.412	0.250	3.5	0.784	0.458	0.0	0.884	0.625	0.0
BadVSFM with WaNet	0.567	0.390	85.5	0.844	0.580	87.0	0.892	0.642	43.6

**Table 2: Performance of backdoor attacks on SAM2 with the LVOS dataset at a 5% poisoning rate across prompts.**

Method	Point			Box			Mask		
	mIoU	J&F	ASR (%)	mIoU	J&F	ASR (%)	mIoU	J&F	ASR (%)
Clean	0.600	0.474	0.0	0.607	0.411	0.0	0.882	0.817	0.0
BadNet	0.508	0.421	0.0	0.749	0.616	0.0	0.881	0.816	0.0
BadVSFM with BadNet	0.575	0.432	94.2	0.875	0.629	92.5	0.920	0.827	46.0
Blended	0.509	0.419	0.0	0.751	0.628	0.0	0.880	0.816	0.0
BadVSFM with Blended	0.591	0.433	95.1	0.842	0.639	94.3	0.894	0.829	64.0
FIBA	0.513	0.430	0.0	0.766	0.640	0.0	0.880	0.816	0.0
BadVSFM with FIBA	0.583	0.441	63.1	0.846	0.654	52.6	0.892	0.828	25.3
WaNet	0.517	0.422	0.0	0.766	0.653	0.0	0.880	0.816	0.0
BadVSFM with WaNet	0.573	0.437	82.3	0.840	0.664	83.1	0.891	0.830	42.3

**Table 3: Gradient cosine statistics between clean and triggered samples on the SAM2 image encoder.**

Method	Mean cos	Median cos	% ( $\cos < 0$ )	% ( $\cos < -0.2$ )	% ( $\cos > 0.2$ )
BadNet	0.285	0.262	4.8%	0.0%	66.2%
BadVSFM with BadNet	-0.214	-0.214	95.2%	51.9%	0.0%

Blended attains the highest ASR on point and box at 92.3% and 86.5% with mIoU around 0.80 to 0.82 and J&F around 0.51 to 0.53, again reflecting substantial gains in attack success with modest movement in utility metrics.

Taken together, across SAM2-Long, BioSAM2, Med-SAM2, and EdgeTAM, BadVSFM consistently raises ASR while maintaining mIoU and J&F, demonstrating that BadVSFM delivers strong backdoor effectiveness without materially compromising clean utility performance.

**Discussion on The Failure of Previous Attacks.** To investigate why traditional backdoor attacks fail on VSFMs, we draw inspiration from prior research on gradient conflicts in backdoor learning [11, 53] and compare the gradient behaviors of BadVSFM and a traditional backdoor attack under clean and triggered samples. Specifically, we use BadNet and BadVSFM with BadNet as our compared methods, and

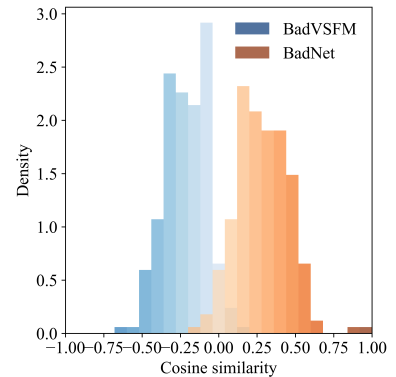
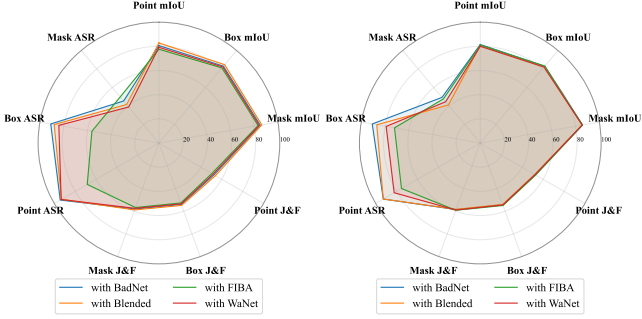


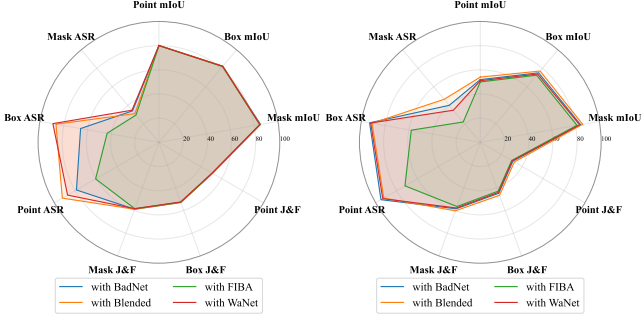
**Figure 4: Cosine similarity distribution of encoder gradients between clean and triggered samples for BadNet and BadVSFM with BadNet.**

evaluate them on SAM2 over the DAVIS dataset under a 5% poisoning rate. For each pair of clean and triggered samples, we perform two separate forward and backward passes, record the gradient vector of the image encoder on the clean sample and on the triggered sample, and then compute the



(a) BioSAM2

(b) MedSAM2

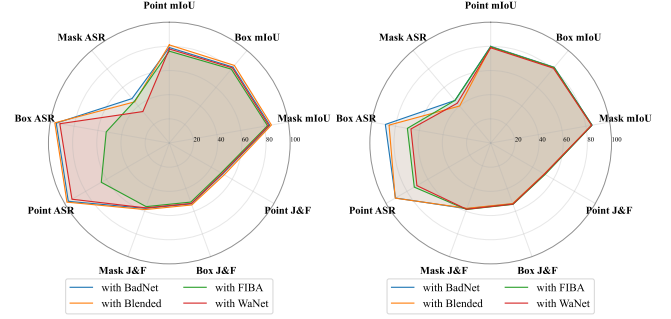


(c) SAM2-Long

(d) EdgeTAM

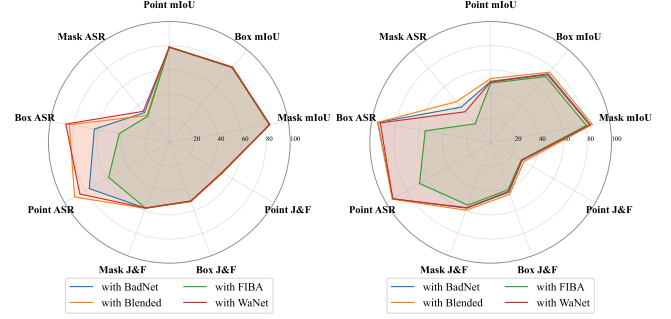
**Figure 5: Backdoor performance for BioSAM2, MedSAM2, SAM2-Long, and EdgeTAM on the DAVIS dataset at a 5% poisoning rate.**

cosine similarity between these two gradients. Table 3 summarizes the main statistics of the encoder gradient cosines for both methods, including the mean, median, and the proportions of pairs falling into several intervals. We observe that, for BadVSFM, the cosine similarity is negative for most sample pairs: both the mean and median are -0.214, 95.2% of the pairs show oppositely oriented gradients, and 51.9% of the pairs exhibit clear and strong conflicts. In contrast, for BadNet, the cosine similarities are predominantly positive: the mean and median lie around 0.262 to 0.285. Only a tiny fraction, 4.8%, of pairs are negatively correlated, and 66.2% of the pairs have highly aligned gradients. These statistics indicate that BadVSFM drives the encoder to update clean and triggered samples in competing directions, effectively pushing their representations apart in the feature space, whereas BadNet keeps the gradients for clean and triggered inputs largely aligned and thus tends to fit both types of samples in a similar way rather than carving out a distinct representation for the trigger. Figure 4 further visualizes the cosine distributions of the two methods as histograms, where we can clearly see that the distribution of BadVSFM is concentrated on the negative half-axis, while that of BadNet is skewed toward the positive half-axis, with minimal overlap between them. This indicates a substantial difference in the gradient geometry induced by the two training schemes and helps explain why a traditional single-stage backdoor like BadNet almost fails to mount an effective attack on a VSFM such as SAM2. In addition, we also visualize the attention maps of BadVSFM with BadNet and BadNet itself; the detailed analysis is provided in Section 6.3.



(a) BioSAM2

(b) MedSAM2



(c) SAM2-Long

(d) EdgeTAM

**Figure 6: Backdoor performance for BioSAM2, MedSAM2, SAM2-Long, and EdgeTAM on the LVOS dataset at a 5% poisoning rate.**

**Table 4: Ablation on training stages for BadVSFM with BadNet at 5% poisoning for SAM2 on DAVIS.**

Method	Point			Box			Mask		
	mIoU	J&F	ASR (%)	mIoU	J&F	ASR (%)	mIoU	J&F	ASR (%)
Stage 1 only	0.389	0.232	<b>94.4</b>	0.726	0.420	<b>94.5</b>	0.865	0.604	39.5
Stage 2 only	0.512	0.354	3.9	0.784	0.535	0.0	0.847	0.610	0.0
Stage 1 + Stage 2	<b>0.556</b>	<b>0.377</b>	93.0	<b>0.852</b>	<b>0.586</b>	92.2	<b>0.895</b>	<b>0.643</b>	<b>48.3</b>

## 6.2 Ablation Study

**Effect of the Training Stages.** As described in Section 4, BadVSFM uses two training stages. To investigate the contribution of each stage, we conduct an ablation study of different training stages using BadVSFM with BadNet trigger on DAVIS using a 5% poisoning rate and point, box, and mask prompts. As shown in Table 4, combining stage 1 and stage 2 yields the strongest clean performance across all prompts, giving the highest mIoU and J&F and the highest ASR on different prompts. Additionally, the results show that conducting only stage 1 training can achieve good backdoor effectiveness but negatively impact clean performance. For instance, only training stage 1 achieves ASR on point and box at 94.4% and 94.5% while clean performance degrades, with mIoU and J&F lower than the two-stage model by 0.167 and 0.145 under the same prompt setting. By contrast, only training stage 2 raises mIoU and J&F compared with training stage 1 alone, yet significantly decreases ASR to 3.9% on the point prompt, indicating a lack of backdoor effectiveness. These results show that both stages are necessary to achieve strong clean utility and backdoor effectiveness.

**Table 5: Stage 2 loss ablation for SAM2 on the DAVIS dataset at 5% poisoning rate.**

Method	Point			Box			Mask		
	mIoU	J&F	ASR (%)	mIoU	J&F	ASR (%)	mIoU	J&F	ASR (%)
BCE + Dice	<b>0.556</b>	<b>0.377</b>	93.0	<b>0.852</b>	<b>0.586</b>	<b>92.2</b>	<b>0.895</b>	<b>0.643</b>	<b>48.3</b>
Dice only	0.418	0.262	93.7	0.800	0.488	61.1	0.883	0.627	31.6
BCE only	0.415	0.257	<b>94.0</b>	0.786	0.473	64.2	0.881	0.627	35.4

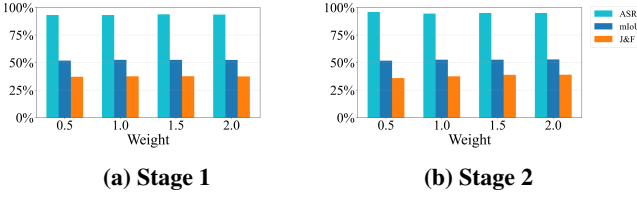


**Figure 7: Ablation of stage 1 (a) and stage 2 (b) loss weights for SAM2 on the DAVIS dataset at 5% poisoning rate.**

**Effect of the Loss Function Weights.** As stated in Section 4, each stage uses two loss coefficients  $\lambda_1$  and  $\lambda_2$ . To assess the sensitivity of BadVSFM to these coefficients, we perform ablations on SAM2 based on the DAVIS dataset with a poisoning rate of 5%. We sweep  $\lambda_1$  and  $\lambda_2$  over 0.5, 1.0, 1.5, and 2.0 under BadVSFM with BadNet on point prompt. For the ablation of stage 1, the results in Figure 7a show only marginal variation when  $\lambda_1$  changes, with ASR at 93%-94%, mIoU at 0.51-0.52, and J&F at 0.37-0.38. Similarly, for stage 2, Figure 7b shows similarly small effects when varying  $\lambda_2$ : ASR at 94%-95%, mIoU at 0.51-0.53, and J&F at 0.35-0.39. These trends suggest that the loss weights across both stages have limited influence on backdoor efficacy and clean performance. Thus, the default setting with  $\lambda_1 = \lambda_2 = 1.0$  is sufficient within the experiments.

**Effect of the Loss Function in Stage 2.** Stage 2 employs BCE and Dice losses, and to explore the contribution of these two losses, we conduct an ablation study to test these two losses using BadVSFM with BadNet trigger on DAVIS using a 5% poisoning rate and point, box, and mask prompts, where the results are shown in Table 5. The results show that combining BCE and Dice losses achieves the highest mIoU and J&F across all prompts, as well as the highest ASR in box and mask prompts, reaching 92.2% and 48.3%, respectively. If only trained with BCE loss, although the point prompt achieves 94.9% ASR, its mIoU and J&F are the lowest, dropping by 0.141 and 0.120 compared with training with BCE and Dice losses under the same prompt settings, indicating a negative impact on clean performance. Only training Dice loss achieves a higher mIoU and J&F than training with BCE only; however, the ASRs for the box and mask prompts are the lowest at 61.1% and 31.6%, indicating insufficient backdoor efficacy. Overall, training with BCE and Dice losses maintains both the strongest backdoor performance while preserving stable clean performance.

**Effect of the Poisoning Rate.** To investigate how the poisoning rate influences BadVSFM, we conduct an ablation study on BadVSFM with BadNet on DAVIS across different poisoning rates at 2%, 5%, 10%, 15% on point, box, and mask

**Table 6: Poisoning-rate ablation on DAVIS for BadVSFM with BadNet across different prompts.**

Poisoning rate (%)	Point			Box			Mask		
	mIoU	J&F	ASR (%)	mIoU	J&F	ASR (%)	mIoU	J&F	ASR (%)
2	0.564	0.388	91.5	0.844	0.582	89.6	0.890	0.640	47.2
5	0.556	0.377	93.0	0.852	0.586	92.2	0.895	0.643	48.3
10	0.571	0.386	95.2	0.851	0.585	93.1	0.894	0.642	63.1
15	0.557	0.379	92.1	0.852	0.587	95.3	0.894	0.642	74.3

prompts. As shown in Table 6, ASR generally rises with a higher poisoning rate. For example, in the box prompt, ASR grows from 89.6% at 2% poisoning rate to 95.3% at 15% poisoning rate, an increase of 5.7%, and on the mask prompt, ASR improves from 47.2% at 2% poisoning rate to 74.3% at 15% poisoning rate, an improvement of 27.1%. Additionally, the utility performance has minor effects across different rates. For instance, in the box prompt, mIoU varies narrowly from 0.844 to 0.852 and J&F from 0.582 to 0.587, and the other two prompts show a similar trend. These results indicate that raising the poisoning rate strengthens the attack while leaving the clean performance effectively stable.

**Different Attack Targets.** To investigate the feasibility of different attack targets, we conduct an ablation on SAM2 using the DAVIS dataset under BadVSFM with BadNet at a 5% poisoning rate with two different targets: deformation and disappearance. For the deformation target, the trigger frame’s objective is to output a centered circle mask whose radius is 18% of the image’s shorter side. For the disappearance target, the output mask for triggered samples is set to all zeros. The results are shown in Table 7, where all targets achieve good backdoor performance and clean utility performance, and the visualization in Figure 8. For example, the disappearance target achieves the highest ASR in 93.0% on point, and the deformation target follows with ASR of 42.0%. Meanwhile, the disappearance target achieves 0.556 mIoU with J&F of 0.377 on point. For the deformation target, points also maintain reasonable performance, with 0.506 mIoU and 0.291 J&F. We also observe that ASR tends to be lower for box and mask prompts than for point prompts.

This is because the box and mask prompts provide much more spatial information than point prompts. A box prompt supplies a fairly tight coordinate region around the object, while a mask prompt directly feeds the full ground-truth object mask into the model. Compared to a single point, these richer and more localized signals provide continuous and vital information to the network about the object. This makes it more challenging to override the output with an attack target. Overall, both targets produce backdoor effects when triggered, while clean segmentation performance remains stable, indicating controllability and robustness across different attack-target settings under varied prompt conditions.

**Different Trigger Position.** To assess whether the location of the trigger affects the effectiveness of the attack, we perform an ablation on DAVIS at a poisoning rate of 5% using SAM2 under BadVSFM with BadNet across six different trigger placements: top left, top right, bottom left, bottom right, center, and a random place. The results in Table 8 show that the ASRs across all locations are high, while clean

**Table 7: Performance under different attack targets on DAVIS across prompts at 5% poisoning rate.**

Attack Target	Point			Box			Mask		
	mIoU	J&F	ASR (%)	mIoU	J&F	ASR (%)	mIoU	J&F	ASR (%)
Deformation	0.506	0.291	42.0	0.789	0.439	38.0	0.892	0.640	14.7
Disappearance	0.556	0.377	93.0	0.852	0.586	92.2	0.895	0.643	48.3

**Table 8: Trigger-location ablation for SAM2 in BadVSFM with BadNet on DAVIS at a 5% poisoning rate across different prompts.**

Trigger location	Point			Box			Mask		
	mIoU	J&F	ASR (%)	mIoU	J&F	ASR (%)	mIoU	J&F	ASR (%)
Random	0.544	0.372	95.4	0.839	0.576	88.5	0.897	0.644	47.6
Top-Left	0.538	0.371	93.8	0.843	0.579	90.7	0.889	0.637	46.0
Top-Right	0.551	0.381	92.8	0.850	0.584	92.5	0.898	0.646	47.5
Bottom-Left	0.553	0.374	92.9	0.846	0.581	91.3	0.892	0.640	46.7
Bottom-Right	0.556	0.377	93.0	0.852	0.586	92.2	0.895	0.643	48.3
Center	0.559	0.379	94.0	0.854	0.588	91.1	0.896	0.644	47.1

metrics remain stable. For example, the trigger with random placement reaches 95.4% ASR for point prompts, 88.5% for box prompts, and 47.6% for mask prompts. The corresponding mIoU and J&F are 0.544 and 0.372 for point, 0.839 and 0.576 for box, and 0.897 and 0.644 for mask. Across different placements, the ASR varies only slightly, ranging from 92.8% to 95.4% for the point and from 46.0% to 49.6% for the mask. By contrast, the box shows a wider ASR range from 88.5% to 92.5%, while the clean metrics remain tight with mIoU fluctuating by about 0.9% to 2.1% and J&F by about 0.9% to 1.2%. These observations indicate that changing the trigger’s placement has a limited impact on the effectiveness of the backdoor, and BadVSFM remains robust to different trigger placements.

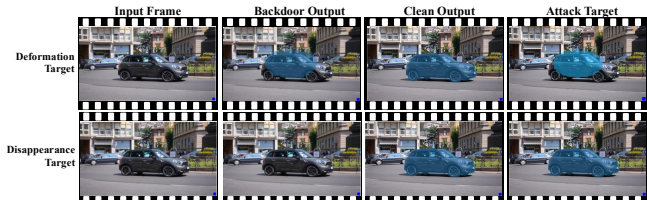


**Figure 8: Visualization of results under different attack targets.**

**Real-world Object as Trigger.** Previous work [14, 49] demonstrates that real-world objects can serve as practical backdoor triggers by altering the associated ground-truth labels, thereby increasing stealth. Building on this idea, we examine whether BadVSFM can exploit physical triggers without hand-crafted patches. Following the physical-trigger construction in [56], we modify DAVIS frames by procedurally generating an object of a given category in the lower-left region of each frame, so that the trigger appears as a natural part of the scene rather than an artificial overlay. For each chosen category, “Leaf”, “Traffic cone”, and “Baseball”, we insert a realistic instance of the object, and evaluate the resulting behavior.

The results are reported in Table 9, and the visualizations are presented in Figure 9. Across the three real-world trig-

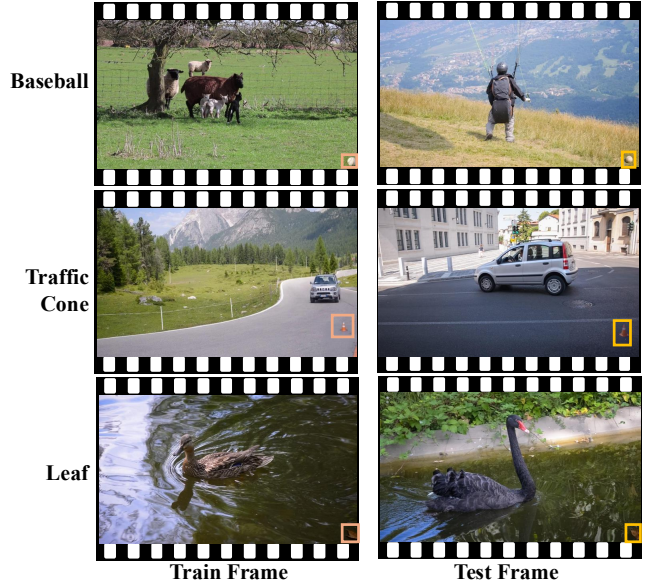


**Figure 9: Visualization of the physical trigger in poisoned frames from the DAVIS dataset.**

**Table 9: Attack performance using real-world objects as triggers on the DAVIS dataset at 5% poisoning rate on point.**

Trigger	ASR (%)	mIoU	J&F
Leaf	93.7	0.550	0.363
Traffic cone	91.3	0.570	0.374
Baseball	92.2	0.562	0.369

gers, the backdoor activates reliably while clean utility remains largely intact. For example, “Leaf” attains 93.7% ASR with 0.550 mIoU and 0.363 J&F, “Traffic cone”, reaches 91.3% ASR with 0.570 mIoU and 0.374 J&F, and “Baseball” achieves 92.2% ASR with 0.562 mIoU and 0.369 J&F. These outcomes indicate that BadVSFM can leverage natural objects as effective physical triggers without sacrificing segmentation quality. Overall, ASR stays in the 91.2%-93.7% band. The clean metrics remain in a narrow range around mIoU 0.55 to 0.57 and J&F 0.36 to 0.37, indicating that BadVSFM can leverage natural, physically plausible triggers while preserving segmentation quality. In sum, BadVSFM paired with real-world triggers substantially elevates the stealth and the potential harm of backdoor attacks in practical settings. Since the trigger is a plausible, naturally occurring object rather than a synthetic patch, mainstream backdoor detection methods fail to localize or flag it.

### 6.3 Interpretability Analysis

**Attention behavior of BadVSFM.** To evaluate the interpretability of BadVSFM, we visualize the image-encoder attention maps of a SAM2 model trained with BadVSFM under the BadNet setting, and compare trigger frames and their clean counterparts using attention rollout [2] in Figure 11. The figure shows three example pairs: in each pair, the trigger frame and its attention map are on the left, and the corre-

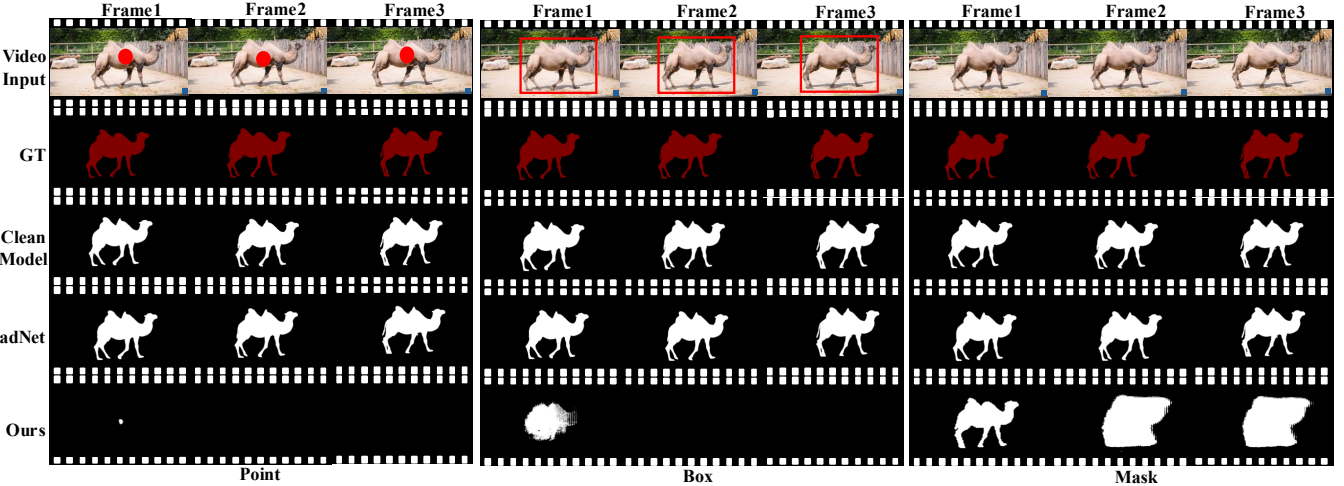


**Figure 10:** Visualization result under three prompt types (Point, Box, and Mask). Each block shows three consecutive frames (top row: video input with prompt); the rows below give ground truth, SAM2 output on clean input, output under the BadNet baseline, and output under our method.

**Table 10:** Defense methods’ performances on BadVSFM with BadNet on DAVIS dataset across different prompts.

		Defense Method								
		without defense	Spectral Signatures	STRIP	Pruning (5 ch.)	Pruning (15 ch.)	Pruning (30 ch.)	Fine-tuning (1% data)	Fine-tuning (5% data)	Fine-tuning (10% data)
Point	mIoU	0.556	0.820	0.834	0.544	0.537	0.538	0.655	0.778	0.784
	J&F	0.377	0.548	0.565	0.364	0.360	0.364	0.422	0.469	0.470
	ASR (%)	93.0	97.9	97.9	91.5	92.9	98.2	97.4	97.9	97.8
Box	mIoU	0.852	0.866	0.876	0.850	0.844	0.843	0.860	0.810	0.804
	J&F	0.586	0.590	0.599	0.575	0.571	0.574	0.562	0.491	0.485
	ASR (%)	92.2	88.8	92.2	92.3	92.3	96.6	90.8	98.3	98.4
Mask	mIoU	0.895	0.890	0.891	0.894	0.888	0.888	0.891	0.886	0.885
	J&F	0.643	0.623	0.624	0.631	0.627	0.627	0.626	0.608	0.605
	ASR (%)	48.3	53.2	53.0	46.7	47.7	42.4	49.3	44.4	44.1

sponding clean frame and its attention map are on the right. All examples are taken from the DAVIS test split with a 5% poisoning rate during training. Following [2], we collect the per-head self-attention from all encoder layers, upsample each map to the finest token grid, apply residual rollout, and then average over heads and queries to obtain a single full-frame heatmap. We overlay this heatmap on the RGB image using percentile clipping and alpha blending, so warmer colors indicate regions with stronger aggregated attention. In the trigger frames, the heatmaps consistently show a pronounced peak at the bottom-right patch where the trigger is located; this bright, high-attention region is small and localized exactly where the trigger patch is placed. In the corresponding clean frames, where the trigger is absent, the attention shifts away from that region and instead concentrates on task-relevant content: responses increase along object boundaries and textured areas, while broad, uniform background regions receive substantially lower attention. Overall, these visualizations indicate that the trigger reliably attracts the encoder’s attention when present, whereas in clean conditions, the model primarily attends to the foreground objects and other semantically meaningful regions.

**Attention behavior of BadNet.** We further compare this behavior with the traditional BadNet by visualizing its encoder

attention map on triggered and clean frames in Figure 12. Unlike BadVSFM, the BadNet shows almost identical attention maps for the triggered and clean inputs. The heatmaps for both cases highlight similar regions on the main object and background, with no clear focus on the trigger patch. This suggests that, under traditional BadNet training, the image encoder does not learn a distinct attention pattern for the trigger; instead, triggered and clean frames are processed in a similar way, which is consistent with our gradient analysis showing highly aligned encoder gradients and helps explain why the traditional backdoor attack fails to produce a reliable backdoor effect on SAM2.

## 6.4 Mitigation

Although many existing studies explore backdoor defense and detection techniques in computer vision and natural language processing [10, 17, 28, 30, 31, 42, 45], their applicability to backdoor attacks on VSFMs remains uncertain. While a comprehensive adaptation of existing defenses is beyond the scope of this work, we implement and evaluate four widely used defense techniques on the BadVSFM with BadNet using SAM2: fine-tuning, pruning [31], STRIP [10], and Spectral Signatures [44]. For the fine-tuning defense, we fine-tune the backdoored model for 10 epochs using clean

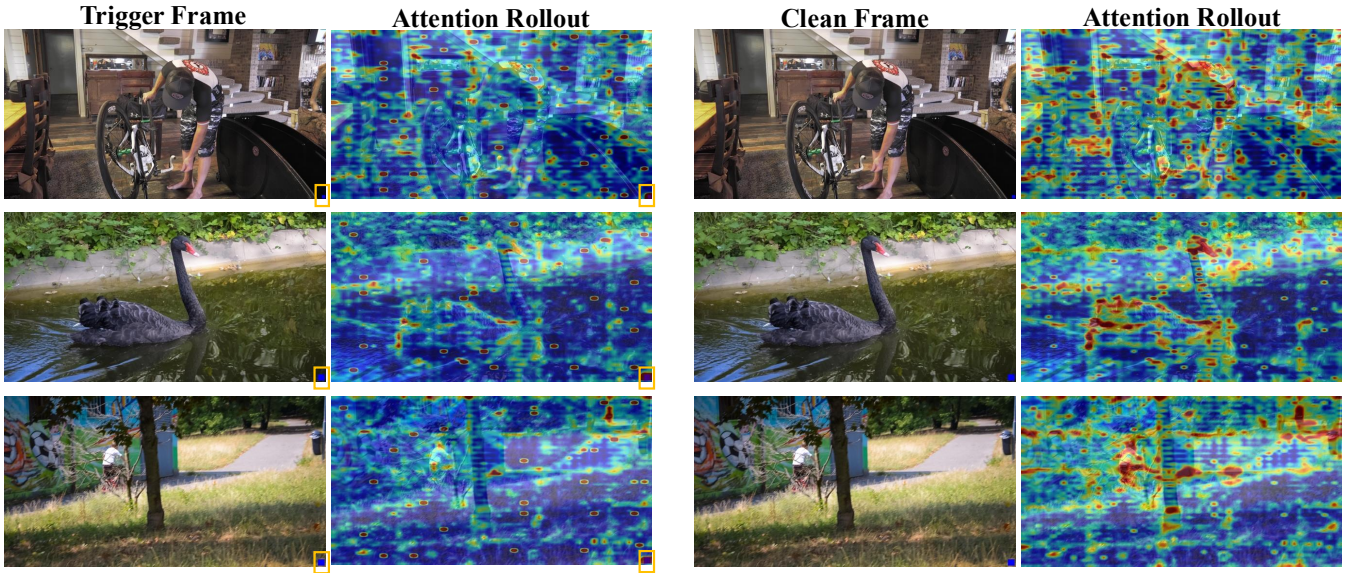


Figure 11: Visualization results for attention maps of the SAM2 image encoder trained with BadVSFM on DAVIS at a 5% poisoning rate.

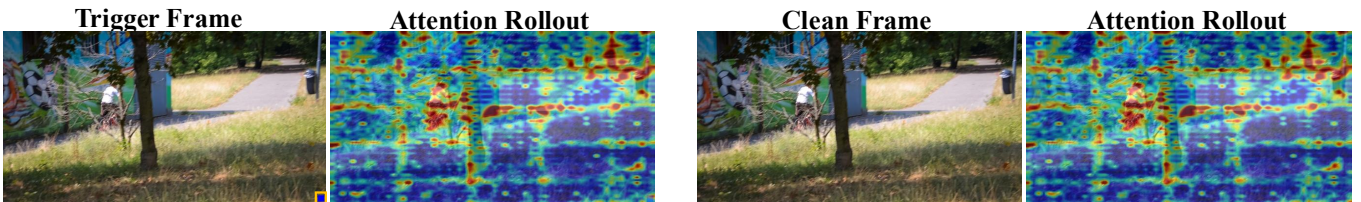


Figure 12: Visualization results for attention maps of the SAM2 image encoder trained with BadNet on DAVIS at a 5% poisoning rate.

training data comprising 1%, 5%, and 10% of the original dataset. For the pruning defense, we follow the original work [31] and prune 5, 15, and 30 channels from the last convolutional layer, respectively. For Spectral Signatures, we adopt a standard implementation to detect and mitigate poisoned signals. For STRIP, we perturb inputs and flag samples whose outputs remain anomalously invariant, indicating potential backdoor samples. As shown in Table 10, none of the defenses substantially weakens the backdoor performance of BadVSFM. For example, after fine-tuning with ten percent clean data, the ASR even increases to 97.8% for point, 98.4% for box, and 44.1% for mask compared with the no-defense method. Meanwhile, Spectral Signatures achieves 88.8% for box, and pruning thirty channels reaches 42.4% for mask, which corresponds to drops of 3.4% and 5.9%, respectively. The ASR reductions are small, and defenses also affect clean utility; for instance, with ten percent fine-tuning, the box mIoU decreases from 0.852 to 0.804 and J&F from 0.586 to 0.485, while the mask mIoU decreases from 0.895 to 0.885 and J&F from 0.643 to 0.605. These results imply that clean-data fine-tuning and channel pruning mostly hurt normal foreground segmentation while leaving the trigger behavior almost unchanged. In addition, Spectral Signatures and STRIP cannot reliably detect BadVSFM because the empty-mask target produces nearly unchanged predictions.

Overall, these results suggest that these four defense tech-

niques are insufficient for countering BadVSFM on VSFMs. Designing more targeted and effective defense strategies for BadVSFM remains a critical research challenge.

## 7 Limitations

We propose the first backdoor attack framework for VSFMs, aiming to reveal their potential security vulnerabilities. Despite the promising results, our study still has several limitations that point to meaningful directions for future work.

- **Limited model coverage.** Our experiments focus on a limited set of video segmentation foundation models. Although these models are representative of current mainstream architectures, they cannot fully capture the diversity of existing or emerging VSFMs designs. Future research should extend our framework to a broader range of architectures and explore whether the attack principles and behaviors observed here generalize to models with different segmentation mechanisms or prompting interfaces.
- **Limited dataset diversity.** The evaluation in this work is conducted mainly on two benchmark datasets, LVOS and DAVIS. These datasets are widely adopted in the video object segmentation community and provide a good starting point for empirical analysis, yet they are

relatively small in scale and have limited scene variety. Future studies could include larger and more diverse datasets to better assess the generality of the attack, including real-world or long-term video sequences with greater variations in motion, illumination, and object appearance.

- **Limited exploration of defense strategies.** We investigate four commonly used defense techniques in deep learning, but all fail to effectively mitigate the proposed attack. This reveals that existing generic defenses are not well-suited for VSFMs, which operate under complex spatiotemporal conditions. Future work could explore defense strategies specifically designed for this domain, such as spatiotemporal anomaly detection, trigger inversion methods tailored for video inputs, or robust training pipelines that enhance the model’s resistance to backdoor threats.

## 8 Conclusion

This work introduces BadVSFM, the first backdoor attack framework tailored to VSFMs for video object segmentation, exposing their security vulnerabilities. We use a two-stage training strategy with effectiveness and utility losses to jointly ensure attack success and preserve clean performance. Stage 1 fine-tunes the image encoder so triggered frames move toward a target embedding while clean frames stay aligned with a reference encoder. Stage 2 updates the mask decoder across prompt types so that triggered frame–prompt pairs map to a shared target mask, while clean masks match a reference decoder. Experiments on DAVIS and LVOS with multiple prompts and trigger patterns show that BadVSFM achieves strong backdoor performance while keeping clean segmentation close to the original model. Ablation studies over loss terms and weights reveal that both ASR and clean performance remain stable across a broad range, indicating robustness to hyperparameters. Removing either stage 1 training or stage 2 training clearly harms ASR or clean utility, confirming the necessity of the two-stage design. To explain why traditional attacks fail on VSFMs, we analyze gradient conflict and interpretability analysis by drawing attention maps. BadVSFM yields mostly negative cosine similarities between encoder gradients of clean and triggered samples, indicating conflicting updates that separate them, whereas BadNet shows mainly positive similarities and thus fits both together. Attention maps further show that BadVSFM drives triggered inputs to focus on the trigger while clean inputs still attend to true foreground objects. We also test four common defenses (fine-tuning, pruning, Spectral Signatures, STRIP) and find them largely ineffective against BadVSFM, underscoring serious backdoor risks for VSFMs and the need for tailored attack and defense mechanisms. Overall, BadVSFM exposes critical backdoor security risks for mainstream VSFMs in video object segmentation and underscores the need for attack and defense mechanisms explicitly tailored to this emerging model class.

## 9 Ethics Considerations

This study aims to reveal and investigate overlooked security risks in VSFMs, particularly in the context of backdoor attacks. Although the proposed framework, BadVSFM, demonstrates an effective method for implanting backdoors into VSFMs, our intention is not to promote or disseminate malicious attack techniques. Instead, our goal is to raise awareness within the research community about the unique vulnerabilities of VSFMs and to lay the groundwork for building more robust, interpretable, and secure video segmentation systems.

All experiments are conducted responsibly in controlled environments using publicly available datasets such as LVOS and DAVIS. We do not release any poisoned models or datasets with triggers. No human data or privacy-sensitive information is involved in this study. In future work, we plan to explore effective defense mechanisms and detection techniques for VSFMs, aiming to enhance the reliability and security of these powerful models before their deployment in safety-critical applications, such as autonomous driving, medical imaging, and robotics.

## References

- [1] Cvpr 2018 wad video segmentation challenge (autonomous driving). Kaggle competition, 2018. [4](#)
- [2] Samira Abnar and Willem H. Zuidema. Quantifying attention flow in transformers. In Dan Jurafsky, Joyce Chai, Natalie Schluter, and Joel R. Tetraeault, editors, *Proceedings of the 58th Annual Meeting of the Association for Computational Linguistics, ACL 2020, Online, July 5-10, 2020*, pages 4190–4197. Association for Computational Linguistics, 2020. doi: 10.18653/V1/2020.ACL-MAIN.385. URL <https://doi.org/10.18653/v1/2020.acl-main.385>. [10, 11](#)
- [3] Thomas Brox and Jitendra Malik. Object segmentation by long term analysis of point trajectories. In Kostas Daniilidis, Petros Maragos, and Nikos Paragios, editors, *Computer Vision - ECCV 2010 - 11th European Conference on Computer Vision, Heraklion, Crete, Greece, September 5-11, 2010, Proceedings, Part V*, volume 6315 of *Lecture Notes in Computer Science*, pages 282–295. Springer, 2010. doi: 10.1007/978-3-642-15555-0\_21. URL [https://doi.org/10.1007/978-3-642-15555-0\\_21](https://doi.org/10.1007/978-3-642-15555-0_21). [3](#)
- [4] Sergi Caelles, Kevis-Kokitsi Maninis, Jordi Pont-Tuset, Laura Leal-Taixé, Daniel Cremers, and Luc Van Gool. One-shot video object segmentation. In *2017 IEEE Conference on Computer Vision and Pattern Recognition, CVPR 2017, Honolulu, HI, USA, July 21-26, 2017*, pages 5320–5329. IEEE Computer Society, 2017. [3](#)
- [5] Xinyun Chen, Chang Liu, Bo Li, Kimberly Lu, and Dawn Song. Targeted backdoor attacks on deep learning systems using data poisoning. *CoRR*, abs/1712.05526, 2017. [2](#)

- [6] Zhen Chen, Zongming Zhang, Wenwu Guo, Xingjian Luo, Long Bai, Jinlin Wu, Hongliang Ren, and Hongbin Liu. Asi-seg: Audio-driven surgical instrument segmentation with surgeon intention understanding. In *IEEE/RSJ International Conference on Intelligent Robots and Systems, IROS 2024, Abu Dhabi, United Arab Emirates, October 14-18, 2024*, pages 13773–13779. IEEE, 2024. 2
- [7] Shuangrui Ding, Rui Qian, Xiaoyi Dong, Pan Zhang, Yuhang Zang, Yuhang Cao, Yuwei Guo, Dahu Lin, and Jiaqi Wang. Sam2long: Enhancing SAM 2 for long video segmentation with a training-free memory tree. *CoRR*, abs/2410.16268, 2024. doi: 10.48550/ARXIV.2410.16268. URL <https://doi.org/10.48550/arXiv.2410.16268>. 5, 6
- [8] Alon Faktor and Michal Irani. Video segmentation by non-local consensus voting. In Michel François Valstar, Andrew P. French, and Tony P. Pridmore, editors, *British Machine Vision Conference, BMVC 2014, Nottingham, UK, September 1-5, 2014*. BMVA Press, 2014. URL <https://bmva-archive.org.uk/bmvc/2014/papers/paper008/index.html>. 3
- [9] Yu Feng, Benteng Ma, Jing Zhang, Shanshan Zhao, Yong Xia, and Dacheng Tao. FIBA: frequency-injection based backdoor attack in medical image analysis. In *IEEE/CVF Conference on Computer Vision and Pattern Recognition, CVPR 2022, New Orleans, LA, USA, June 18-24, 2022*, pages 20844–20853. IEEE, 2022. doi: 10.1109/CVPR52688.2022.02021. URL <https://doi.org/10.1109/CVPR52688.2022.02021>. 3, 4, 5, 6
- [10] Yansong Gao, Chang Xu, Derui Wang, Shiping Chen, Damith Chinthana Ranasinghe, and Surya Nepal. STRIP: a defence against trojan attacks on deep neural networks. In David M. Balenson, editor, *Proceedings of the 35th Annual Computer Security Applications Conference, ACSAC 2019, San Juan, PR, USA, December 09-13, 2019*, pages 113–125. ACM, 2019. 2, 11
- [11] Naibin Gu, Peng Fu, Xiyu Liu, Zhengxiao Liu, Zheng Lin, and Weiping Wang. A gradient control method for backdoor attacks on parameter-efficient tuning. In Anna Rogers, Jordan L. Boyd-Graber, and Naoaki Okazaki, editors, *Proceedings of the 61st Annual Meeting of the Association for Computational Linguistics (Volume 1: Long Papers), ACL 2023, Toronto, Canada, July 9-14, 2023*, pages 3508–3520. Association for Computational Linguistics, 2023. doi: 10.18653/V1/2023.ACL-LONG.194. URL <https://doi.org/10.18653/v1/2023.acl-long.194>. 7
- [12] Tianyu Gu, Brendan Dolan-Gavitt, and Siddharth Garg. Badnets: Identifying vulnerabilities in the machine learning model supply chain. *CoRR*, abs/1708.06733, 2017. 2, 3, 4, 5, 6
- [13] Jihui Guo, Zongmin Zhang, Zhen Sun, Yuhao Yang, Jinlin Wu, Fu Zhang, and Xinlei He. 6dattack: Backdoor attacks in the 6dof pose estimation. In *AAAI Conference on Artificial Intelligence (AAAI)*, 2026. 3
- [14] Xingshuo Han, Guowen Xu, Yuan Zhou, Xuehuan Yang, Jiwei Li, and Tianwei Zhang. Physical backdoor attacks to lane detection systems in autonomous driving. In João Magalhães, Alberto Del Bimbo, Shin’ichi Satoh, Nicu Sebe, Xavier Alameda-Pineda, Qin Jin, Vincent Oria, and Laura Toni, editors, *MM ’22: The 30th ACM International Conference on Multimedia, Lisboa, Portugal, October 10 - 14, 2022*, pages 2957–2968. ACM, 2022. 10
- [15] Xinlei He, Guowen Xu, Xingshuo Han, Qian Wang, Lingchen Zhao, Chao Shen, Chenhao Lin, Zhengyu Zhao, Qian Li, Le Yang, Shouling Ji, Shaofeng Li, Haojin Zhu, Zhibo Wang, Rui Zheng, Tianqing Zhu, Qi Li, Chaoxiang He, Qifan Wang, Hongsheng Hu, Shuo Wang, Shi-Feng Sun, Hongwei Yao, Zhan Qin, Kai Chen, Yue Zhao, Hongwei Li, Xinyi Huang, and Dengguo Feng. Artificial intelligence security and privacy: a survey. *Science China Information Sciences*, 2025. 2, 3
- [16] Lingyi Hong, Wenchao Chen, Zhongying Liu, Wei Zhang, Pinxue Guo, Zhaoyu Chen, and Wenqiang Zhang. LVOS: A benchmark for long-term video object segmentation. In *IEEE/CVF International Conference on Computer Vision, ICCV 2023, Paris, France, October 1-6, 2023*, pages 13434–13446. IEEE, 2023. doi: 10.1109/ICCV51070.2023.01240. URL <https://doi.org/10.1109/ICCV51070.2023.01240>. 2, 4, 5, 6
- [17] Kunzhe Huang, Yiming Li, Baoyuan Wu, Zhan Qin, and Kui Ren. Backdoor defense via decoupling the training process. In *The Tenth International Conference on Learning Representations, ICLR 2022, Virtual Event, April 25-29, 2022*. OpenReview.net, 2022. 11
- [18] Fabian Isensee, Jens Petersen, André Klein, David Zimmerer, Paul F. Jaeger, Simon Kohl, Jakob Wasserthal, Gregor Köhler, Tobias Norajitra, Sebastian J. Wirkert, and Klaus H. Maier-Hein. Abstract: nnu-net: Self-adapting framework for u-net-based medical image segmentation. In Heinz Handels, Thomas M. Deserno, Andreas K. Maier, Klaus Hermann Maier-Hein, Christoph Palm, and Thomas Tolxdorff, editors, *Bildverarbeitung für die Medizin 2019 - Algorithmen - Systeme - Anwendungen. Proceedings des Workshops vom 17. bis 19. März 2019 in Lübeck*, Informatik Aktuell, page 22. Springer Vieweg, 2019. 2
- [19] Suyog Dutt Jain and Kristen Grauman. Supervoxel-consistent foreground propagation in video. In David J. Fleet, Tomás Pajdla, Bernt Schiele, and Tinne Tuytelaars, editors, *Computer Vision - ECCV 2014 - 13th European Conference, Zurich, Switzerland, September 6-12, 2014, Proceedings, Part IV*, volume 8692

- of *Lecture Notes in Computer Science*, pages 656–671. Springer, 2014. doi: 10.1007/978-3-319-10593-2\_43. URL [https://doi.org/10.1007/978-3-319-10593-2\\_43](https://doi.org/10.1007/978-3-319-10593-2_43). 3
- [20] Zhang Jiaxing and Tang Hao. SAM2 for image and video segmentation: A comprehensive survey. *CoRR*, abs/2503.12781, 2025. 1, 6
- [21] Alexander Kirillov, Eric Mintun, Nikhila Ravi, Hanzi Mao, Chloé Rolland, Laura Gustafson, Tete Xiao, Spencer Whitehead, Alexander C. Berg, Wan-Yen Lo, Piotr Dollár, and Ross B. Girshick. Segment anything. In *IEEE/CVF International Conference on Computer Vision, ICCV 2023, Paris, France, October 1-6, 2023*, pages 3992–4003. IEEE, 2023. 3
- [22] Keita Kurita, Paul Michel, and Graham Neubig. Weight poisoning attacks on pretrained models. In Dan Jurafsky, Joyce Chai, Natalie Schluter, and Joel R. Tetraeault, editors, *Proceedings of the 58th Annual Meeting of the Association for Computational Linguistics, ACL 2020, Online, July 5-10, 2020*, pages 2793–2806. Association for Computational Linguistics, 2020. 3
- [23] Fuxin Li, Taeyoung Kim, Ahmad Humayun, David Tsai, and James M. Rehg. Video segmentation by tracking many figure-ground segments. In *IEEE International Conference on Computer Vision, ICCV 2013, Sydney, Australia, December 1-8, 2013*, pages 2192–2199. IEEE Computer Society, 2013. doi: 10.1109/ICCV.2013.273. URL <https://doi.org/10.1109/ICCV.2013.273>. 4
- [24] Kaiyu Li, Ruixun Liu, Xiangyong Cao, Xueru Bai, Feng Zhou, Deyu Meng, and Zhi Wang. Segearthov: Towards training-free open-vocabulary segmentation for remote sensing images. In *IEEE/CVF Conference on Computer Vision and Pattern Recognition, CVPR 2025, Nashville, TN, USA, June 11-15, 2025*, pages 10545–10556. Computer Vision Foundation / IEEE, 2025. 2
- [25] Yuezun Li, Yiming Li, Baoyuan Wu, Longkang Li, Ran He, and Siwei Lyu. Invisible backdoor attack with sample-specific triggers. In *2021 IEEE/CVF International Conference on Computer Vision, ICCV 2021, Montreal, QC, Canada, October 10-17, 2021*, pages 16443–16452. IEEE, 2021. 2, 3, 4, 5, 6
- [26] Yifan Liao, Yuxin Cao, Yedi Zhang, Wentao He, Yan Xiao, Xianglong Du, Zhiyong Huang, and Jin Song Dong. Towards stealthy and effective backdoor attacks on lane detection: A naturalistic data poisoning approach. *CoRR*, abs/2508.15778, 2025. doi: 10.48550/ARXIV.2508.15778. URL <https://doi.org/10.48550/arXiv.2508.15778>. 3
- [27] Taegyu Lim, Seunghoon Hong, Bohyung Han, and Joon Hee Han. Joint segmentation and pose tracking of human in natural videos. In *IEEE International Conference on Computer Vision, ICCV 2013, Sydney, Australia, December 1-8, 2013*, pages 833–840. IEEE Computer Society, 2013. doi: 10.1109/ICCV.2013.108. URL <https://doi.org/10.1109/ICCV.2013.108>. 3
- [28] Kang Liu, Brendan Dolan-Gavitt, and Siddharth Garg. Fine-pruning: Defending against backdooring attacks on deep neural networks. In Michael D. Bailey, Thorsten Holz, Manolis Stamatogiannakis, and Sotiris Ioannidis, editors, *Research in Attacks, Intrusions, and Defenses - 21st International Symposium, RAID 2018, Heraklion, Crete, Greece, September 10-12, 2018, Proceedings*, volume 11050 of *Lecture Notes in Computer Science*, pages 273–294. Springer, 2018. 11
- [29] Sihan Liu, Yiwei Ma, Xiaoqing Zhang, Haowei Wang, Jiayi Ji, Xiaoshuai Sun, and Rongrong Ji. Rotated multi-scale interaction network for referring remote sensing image segmentation. In *IEEE/CVF Conference on Computer Vision and Pattern Recognition, CVPR 2024, Seattle, WA, USA, June 16-22, 2024*, pages 26648–26658. IEEE, 2024. 2
- [30] Yule Liu, Zhen Sun, Xinlei He, and Xinyi Huang. Quantized delta weight is safety keeper. *CoRR*, abs/2411.19530, 2024. 11
- [31] Yuntao Liu, Yang Xie, and Ankur Srivastava. Neural trojans. *CoRR*, abs/1710.00942, 2017. 2, 11, 12
- [32] Jialin Lu, Junjie Shan, Ziqi Zhao, and Ka-Ho Chow. Anywheredoor: Multi-target backdoor attacks on object detection. *CoRR*, abs/2411.14243, 2024. 3
- [33] Jie Lv, Haonan Tong, Qiang Pan, Zhilong Zhang, Xinxin He, Tao Luo, and Changchuan Yin. Importance-aware image segmentation-based semantic communication for autonomous driving. *CoRR*, abs/2401.10153, 2024. 2
- [34] Jieru Mei, Alex Zihao Zhu, Xinchen Yan, Hang Yan, Siyuan Qiao, Liang-Chieh Chen, and Henrik Kretzschmar. Waymo open dataset: Panoramic video panoptic segmentation. In Shai Avidan, Gabriel J. Brostow, Moustapha Cissé, Giovanni Maria Farinella, and Tal Hassner, editors, *Computer Vision - ECCV 2022 - 17th European Conference, Tel Aviv, Israel, October 23-27, 2022, Proceedings, Part XXIX*, volume 13689 of *Lecture Notes in Computer Science*, pages 53–72. Springer, 2022. 4
- [35] Tuan Anh Nguyen and Anh Tuan Tran. Wanet - imperceptible warping-based backdoor attack. In *9th International Conference on Learning Representations, ICLR 2021, Virtual Event, Austria, May 3-7, 2021*. OpenReview.net, 2021. 4, 5, 6
- [36] Federico Perazzi, Anna Khoreva, Rodrigo Benenson, Bernt Schiele, and Alexander Sorkine-Hornung. Learning video object segmentation from static images. In

- 2017 IEEE Conference on Computer Vision and Pattern Recognition, CVPR 2017, Honolulu, HI, USA, July 21-26, 2017*, pages 3491–3500. IEEE Computer Society, 2017. doi: 10.1109/CVPR.2017.372. URL <https://doi.org/10.1109/CVPR.2017.372>. 3
- [37] Jordi Pont-Tuset, Federico Perazzi, Sergi Caelles, Pablo Arbeláez, Alexander Sorkine-Hornung, and Luc Van Gool. The 2017 DAVIS challenge on video object segmentation. *CoRR*, abs/1704.00675, 2017. URL <http://arxiv.org/abs/1704.00675>. 2, 4, 5, 6
- [38] Nikhila Ravi, Valentin Gabeur, Yuan-Ting Hu, Ronghang Hu, Chaitanya Ryali, Tengyu Ma, Haitham Khedr, Roman Rädle, Chloé Rolland, Laura Gustafson, Eric Mintun, Junting Pan, Kalyan Vasudev Alwala, Nicolas Carion, Chao-Yuan Wu, Ross B. Girshick, Piotr Dollár, and Christoph Feichtenhofer. SAM 2: Segment anything in images and videos. In *The Thirteenth International Conference on Learning Representations, ICLR 2025, Singapore, April 24-28, 2025*. OpenReview.net, 2025. URL <https://openreview.net/forum?id=Ha6RTeWMd0>. 1, 3, 5
- [39] Meta AI Research. Sam2: Segment anything model 2. <https://github.com/facebookresearch/sam2>, 2024. Accessed: 2025-08-05. 3, 5
- [40] Lei Sun, Kailun Yang, Xinxin Hu, Weijian Hu, and Kaiwei Wang. Real-time fusion network for RGB-D semantic segmentation incorporating unexpected obstacle detection for road-driving images. *IEEE Robotics Autom. Lett.*, 5(4):5558–5565, 2020. 2
- [41] Zhen Sun, Huan Xu, Jinlin Wu, Zhen Chen, Hongbin Liu, and Zhen Lei. Pwseg: Weakly-supervised surgical instrument instance segmentation. In *IEEE International Conference on Image Processing, ICIP 2024, Abu Dhabi, United Arab Emirates, october 27-30, 2024*, pages 3144–3150. IEEE, 2024. 2
- [42] Zhen Sun, Tianshuo Cong, Yule Liu, Chenhao Lin, Xinlei He, Rongmao Chen, Xingshuo Han, and Xinyi Huang. Peftguard: Detecting backdoor attacks against parameter-efficient fine-tuning. In *IEEE Symposium on Security and Privacy, SP 2025, San Francisco, CA, USA, May 12-15, 2025*, pages 1713–1731. IEEE, 2025. 2, 3, 11
- [43] Marvin Teichmann, Michael Weber, J. Marius Zöllner, Roberto Cipolla, and Raquel Urtasun. Multinet: Real-time joint semantic reasoning for autonomous driving. In *2018 IEEE Intelligent Vehicles Symposium, IV 2018, Changshu, Suzhou, China, June 26-30, 2018*, pages 1013–1020. IEEE, 2018. 2
- [44] Brandon Tran, Jerry Li, and Aleksander Madry. Spectral signatures in backdoor attacks. In Samy Bengio, Hanna M. Wallach, Hugo Larochelle, Kristen Grauman, Nicolò Cesa-Bianchi, and Roman Garnett, editors, *Advances in Neural Information Processing Systems 31: Annual Conference on Neural Information Processing Systems 2018, NeurIPS 2018, December 3-8, 2018, Montréal, Canada*, pages 8011–8021, 2018. URL <https://proceedings.neurips.cc/paper/2018/hash/280cf18baf4311c92aa5a042336587d3-Abstract.html>. 2, 11
- [45] Bolun Wang, Yuanshun Yao, Shawn Shan, Huiying Li, Bimal Viswanath, Haitao Zheng, and Ben Y. Zhao. Neural cleanse: Identifying and mitigating backdoor attacks in neural networks. In *2019 IEEE Symposium on Security and Privacy, SP 2019, San Francisco, CA, USA, May 19-23, 2019*, pages 707–723. IEEE, 2019. 11
- [46] Lijin Wang, Jingjing Wang, Tianshuo Cong, Xinlei He, Zhan Qin, and Xinyi Huang. From purity to peril: Backdooring merged models from “harmless” benign components. In *USENIX Security Symposium (USENIX Security)*, 2025. 3
- [47] Ruotong Wang, Mingli Zhu, Jiarong Ou, Rui Chen, Xin Tao, Pengfei Wan, and Baoyuan Wu. Badvideo: Stealthy backdoor attack against text-to-video generation. *CoRR*, abs/2504.16907, 2025. 3
- [48] Tong Wang, Yuan Yao, Feng Xu, Shengwei An, Hanghang Tong, and Ting Wang. Backdoor attack through frequency domain. *CoRR*, abs/2111.10991, 2021. 3
- [49] Emily Wenger, Josephine Passananti, Arjun Nitin Bhagoji, Yuanshun Yao, Haitao Zheng, and Ben Y. Zhao. Backdoor attacks against deep learning systems in the physical world. In *IEEE Conference on Computer Vision and Pattern Recognition, CVPR 2021, virtual, June 19-25, 2021*, pages 6206–6215. Computer Vision Foundation / IEEE, 2021. doi: 10.1109/CVPR46437.2021.00614. URL [https://openaccess.thecvf.com/content/CVPR2021/html/Wenger\\_Backdoor\\_Attacks\\_Against\\_Deep\\_Learning\\_Systems\\_in\\_the\\_Physical\\_World\\_CVPR\\_2021\\_paper.html](https://openaccess.thecvf.com/content/CVPR2021/html/Wenger_Backdoor_Attacks_Against_Deep_Learning_Systems_in_the_Physical_World_CVPR_2021_paper.html). 10
- [50] Ning Xu, Linjie Yang, Yuchen Fan, Dingcheng Yue, Yuchen Liang, Jianchao Yang, and Thomas S. Huang. Youtube-vos: A large-scale video object segmentation benchmark. *CoRR*, abs/1809.03327, 2018. 4
- [51] Zhiling Yan, Weixiang Sun, Rong Zhou, Zhengqing Yuan, Kai Zhang, Yiwei Li, Tianming Liu, Quanzheng Li, Xiang Li, Lifang He, and Lichao Sun. Biomedical SAM 2: Segment anything in biomedical images and videos. *CoRR*, abs/2408.03286, 2024. 1, 3
- [52] Rui Yao, Guosheng Lin, Shixiong Xia, Jiaqi Zhao, and Yong Zhou. Video object segmentation and tracking: A survey. *ACM Trans. Intell. Syst. Technol.*, 11(4):36:1–36:47, 2020. 1, 2
- [53] Tianhe Yu, Saurabh Kumar, Abhishek Gupta, Sergey Levine, Karol Hausman, and Chelsea Finn. Gradient surgery for multi-task learning. In Hugo

- Larochelle, Marc’Aurelio Ranzato, Raia Hadsell, Maria-Florina Balcan, and Hsuan-Tien Lin, editors, *Advances in Neural Information Processing Systems 33: Annual Conference on Neural Information Processing Systems 2020, NeurIPS 2020, December 6-12, 2020, virtual*, 2020. URL <https://proceedings.neurips.cc/paper/2020/hash/3fe78a8acf5fda99de95303940a2420c-Abstract.html>. 7
- [54] Hangtao Zhang, Shengshan Hu, Yichen Wang, Leo Yu Zhang, Ziqi Zhou, Xianlong Wang, Yanjun Zhang, and Chao Chen. Detector collapse: Backdooring object detection to catastrophic overload or blindness in the physical world. In *Proceedings of the Thirty-Third International Joint Conference on Artificial Intelligence, IJCAI 2024, Jeju, South Korea, August 3-9, 2024*, pages 1670–1678. ijcai.org, 2024. 3
- [55] Mingya Zhang, Liang Wang, Zhihao Chen, Yiyuan Ge, and Xianping Tao. Path-sam2: Transfer sam2 for digital pathology semantic segmentation. 2024. URL <https://api.semanticscholar.org/CorpusID:271745331>. 1
- [56] Haozhe Zhao, Xiaojian (Shawn) Ma, Liang Chen, Shuzheng Si, Ruijie Wu, Kaikai An, Peiyu Yu, Minjia Zhang, Qing Li, and Baobao Chang. Ultraedit: Instruction-based fine-grained image editing at scale. In Amir Globersons, Lester Mackey, Danielle Belgrave, Angela Fan, Ulrich Paquet, Jakub M. Tomczak, and Cheng Zhang, editors, *Advances in Neural Information Processing Systems 38: Annual Conference on Neural Information Processing Systems 2024, NeurIPS 2024, Vancouver, BC, Canada, December 10 - 15, 2024*. URL [http://papers.nips.cc/paper\\_files/paper/2024/hash/05a30a0fc9e6bacdd3abd4ca8508a9e6-Abstract-Datasets\\_and\\_Benchmarks\\_Track.html](http://papers.nips.cc/paper_files/paper/2024/hash/05a30a0fc9e6bacdd3abd4ca8508a9e6-Abstract-Datasets_and_Benchmarks_Track.html). 10
- [57] Shihao Zhao, Xingjun Ma, Xiang Zheng, James Bailey, Jingjing Chen, and Yu-Gang Jiang. Clean-label backdoor attacks on video recognition models. In *2020 IEEE/CVF Conference on Computer Vision and Pattern Recognition, CVPR 2020, Seattle, WA, USA, June 13-19, 2020*, pages 14431–14440. Computer Vision Foundation / IEEE, 2020. 3
- [58] Zhiyuan Zhong, Zhen Sun, Yepang Liu, Xinlei He, and Guanhong Tao. Backdoor attack on vision language models with stealthy semantic manipulation. *CoRR*, abs/2506.07214, 2025. 3
- [59] Chong Zhou, Chenchen Zhu, Yunyang Xiong, Saksham Suri, Fanyi Xiao, Lemeng Wu, Raghuraman Krishnamoorthi, Bo Dai, Chen Change Loy, Vikas Chandra, and Bilge Soran. Edgetam: On-device track anything model. In *IEEE/CVF Conference on Computer Vision and Pattern Recognition, CVPR 2025, Nashville, TN, USA, June 11-15, 2025*, pages 13832–13842. Computer Vision Foundation / IEEE, 2025. doi: 10.1109/CVPR52734.2025.01291. URL [https://openaccess.thecvf.com/content/CVPR2025/html/Zhou\\_EdgeTAM\\_On-Device\\_TrackAnything\\_Model\\_CVPR\\_2025\\_paper.html](https://openaccess.thecvf.com/content/CVPR2025/html/Zhou_EdgeTAM_On-Device_TrackAnything_Model_CVPR_2025_paper.html). 5, 6
- [60] Jiayuan Zhu, Yunli Qi, and Junde Wu. Medical SAM 2: Segment medical images as video via segment anything model 2. *CoRR*, abs/2408.00874, 2024. 1, 3, 5, 6